

## Radial modes of pressure bumps and dips in astrophysical discs

ARMAND LECLERC <sup>1</sup>, GUILLAUME LAIBE <sup>2</sup>, ELLIOT LYNCH,<sup>2</sup> AND NICOLAS PEREZ<sup>3</sup>

<sup>1</sup>*Institute of Science and Technology Austria (ISTA), Am Campus 1, 3400 Klosterneuburg, Austria*

<sup>2</sup>*ENS de Lyon, CRAL UMR5574, Université Claude Bernard Lyon 1, CNRS, Lyon, F-69007, France*

<sup>3</sup>*Department of Geophysics, Porter school of the Environment and Earth Sciences, Tel Aviv University, 69978 Tel Aviv, Israel*

### ABSTRACT

This study investigates the signatures of pressure extrema on global oscillations in discs. To this end, we use the framework of wave topology to establish a generalised local dispersion relation that includes pressure gradients. We highlight the influence of a previously unrecognized epicyclic–acoustic frequency and derive an analytical criterion for the existence of a branch of modes transiting between the inertial and the pressure bands. We find that pressure extrema consist of wave guides in which such *topological modes* propagate. The fundamental mode trapped at a pressure bump can propagate at all frequencies, allowing it to resonate with any temporal forcing, while the mode associated with a pressure gap propagates at a fixed frequency, propagates with arbitrary vertical phase velocity. These specific features make them attractive candidates for future discoseismology.

*Keywords:* waves — protoplanetary discs — Methods:analytical

### 1. INTRODUCTION

Solids in protoplanetary discs drift towards regions of higher pressure (Safronov 1972). As such, pressure maxima – often called pressure bumps – are privileged places to collect solids and foster planet formation (e.g. Bae et al. 2023; Lesur et al. 2023; Drażkowska et al. 2023), with locating and characterising such features of great interest to the planet formation community. Only dust can be imaged directly, while the gas pressure profile has recently been quantitatively constrained from inverting the mean rotational profile, using high-precision kinematic data of CO emission lines obtained with ALMA (e.g. Pinte et al. 2023). Departures from circular Keplerian motion can arise from pressure gradients, disc eccentricity or inclination, secondary flows, or additional physical processes such as self-gravity, dust dynamics, or magnetic fields (e.g. Teague et al. 2025). These processes and the presence of protoplanets shape the pressure profile of the gas into a structured disc, with pressure bumps and dips. Probing this flow and these processes by a seismic analysis could be achieved with spatially or time-resolved kinematic data: this is the very goal of *discoseismology*, essentially introduced so far to study accretion discs around black holes (Solheim et al. 1998; Tsang and Lai 2009; Tsang and Butsky 2013; Ortega-Rodríguez et al. 2020; Dewberry et al. 2020a,b; Kato 2024). This approach aims at constraining the

structure of the disc not via the mean flow, but through the study of linear perturbations about its equilibrium.

Linear waves and instabilities have a well-established history as mechanisms for forming structures in discs (Toomre 1964; Goldreich and Lynden-Bell 1965a; Lynden-Bell and Ostriker 1967; Papaloizou and Pringle 1985), for instance the spiral arms of galaxies are understood to be density waves (Lin and Shu 1966; Lynden-Bell and Kalnajs 1972). External perturbers can excite both inertial and acoustic waves at Lindblad resonances, where the orbital period of the mean flow is commensurable with the perturbation’s period, which launches waves in the disc (Lindblad 1948; Goldreich and Tremaine 1978, 1979; Lubow and Ogilvie 1998). This occurs in Saturn’s rings, where ring waves in resonance with oscillations of the planet have been observed by Cassini which provided the first and only seismic data of Saturn (Marley 1991; Hedman and Nicholson 2013; Fuller 2014).

While global modes of isothermal and polytropic discs have been widely investigated (Kato and Fukue 1980; Kato 1983; Papaloizou and Pringle 1985; Blaes 1985; Blaes et al. 2006, 2007), the analysis becomes simpler when focusing solely on small-scale perturbations within the shearing-box framework, where the fluid evolution is described in a small cartesian box rotating with the flow (Hill 1878; Goldreich and Lynden-Bell 1965b). This has led to important advances in our understanding

of wave propagation, instabilities, turbulence, angular-momentum transport and planetesimal formation in accretion and protoplanetary discs (e.g. Kato 1978; Goldreich and Tremaine 1980; Balbus and Hawley 1991; Lubow and Pringle 1993; Goodman 1993; Korycansky and Pringle 1995; Ogilvie 1998; Balbus and Hawley 1998; Ogilvie and Lubow 1999; Youdin and Goodman 2005; Johansen et al. 2007; Nelson et al. 2013).

On the other hand, as in the case in stellar seismology (e.g. Aerts et al. 2010), key targets for discoseismology are the large-scale global modes, since they probe the overall structure of the disc and are the easiest to detect. Among these, *topological modes* are especially attractive, since they can be studied and constrained without the need for short-wavelength or local techniques. These modes stem from a topological property of the differential operator that governs their evolution. While such modes have been investigated for decades in condensed-matter physics, their study in hydrodynamics has emerged only recently (Delplace et al. 2017; Perrot et al. 2019; Perez et al. 2022; Parker et al. 2020; Qin and Fu 2023; Perez et al. 2025). Since topological analysis has received little attention in astrophysical fluids to date, characterization of topological modes may enable new methods of probing the structure of interesting objects. The example of topological waves in stars is to this respect particularly instructive. Leclerc et al. (2022) demonstrated that the cancellation of a particular characteristic frequency in stars necessarily gives rise to a topological mode, explaining why  $f$ -branch modes with small harmonic degrees are not confined to the stellar surface. These modes were subsequently shown to remain robust in the presence of convective regions, radiative dissipation, and are excited by convective motions (Leclerc et al. 2024a; Le Saux et al. 2025). They have also been observed to hybridize with  $g$ -modes, providing the most reliable method to date for inferring the rotation rate of the solar core (Le Saux et al. 2025). Stellar rotation was also found to induce topological modes in seismic spectra (Leclerc et al. 2024b).

Building on these developments performed in the stellar context, we aim to address the following questions: do topological modes exist in discs? If so, how are they related to the pressure profile? We address these questions here, and highlight the special properties these modes have, suggesting their interest for protoplanetary discs seismology and dynamics. In Sect. 2, we start by examining the local propagation of waves, by performing a so-called microlocal analysis of the linear wave operator of a simple model of a disc to obtain the local dispersion relation as well as the local polarization relations between the wave fields (Keppeler 2004; Hall

2013; Onuki 2020; Vidal and de Verdière 2024). This is the first time that this method is used in the context of astrophysical discs. In Sect. 3, we exhibit the topological properties of the problem, and predict the existence of topological modes. We then focus on the role of the presence of extrema in the pressure profile in Sect. 4, analysing how they are reflected in the spectrum of large-scale modes. Further extensions of this study are discussed in Sect. 5.

## 2. LOCAL WAVES WITHOUT SHEARING BOX

### 2.1. Epicyclic-acoustic frequency

We consider an unstratified disc made of a non-self-gravitating ideal gas around a star of mass  $M$ . The equations of motion for the velocity  $\mathbf{v}$ , pressure  $p$  and density  $\rho$  are

$$\partial_t \mathbf{v} + (\mathbf{v} \cdot \nabla) \mathbf{v} = -\frac{1}{\rho} \nabla p - \frac{GM}{r^2} \mathbf{e}_r, \quad (1)$$

$$\partial_t \rho + \nabla \cdot (\rho \mathbf{v}) = 0, \quad (2)$$

along with an appropriate energy equation. We restrict our analysis to the case of a circular disc. In cylindrical coordinates  $(r, \theta, z)$ , the equilibrium profile is parametrized by  $\rho = \rho_0(r)$ ,  $p = p_0(r)$ ,  $v = (0, r\Omega(r), 0)$ . Along the radial direction,

$$r\Omega^2 = \frac{1}{\rho_0} \frac{dp_0}{dr} + \frac{GM}{r^2}. \quad (3)$$

We linearly expand the quantities as  $X = X_0 + X'$  in Eqs.(1)-(2), assuming adiabatic axisymmetric perturbations of the gas ( $\delta p = c_s^2 \delta \rho$ ). One obtains (Latter and Papaloizou 2017)

$$\partial_t v'_r = 2\Omega v'_\theta - \frac{1}{\rho_0} \partial_r p' + \frac{p'}{c_s^2 \rho_0^2} \frac{dp_0}{dr}, \quad (4)$$

$$\partial_t v'_\theta = -\left(2\Omega + r \frac{d\Omega}{dr}\right) v'_r, \quad (5)$$

$$\partial_t v'_z = -\frac{1}{\rho_0} \partial_z p', \quad (6)$$

$$\partial_t p' = -p_0 \left( \frac{1}{r} \partial_r (r v'_r) + \partial_z v'_z \right) - \frac{dp_0}{dr} v'_r. \quad (7)$$

We apply the change of variables

$$(v'_r, v'_\theta, v'_z) \mapsto \mathbf{u} \equiv \sqrt{r\rho_0} \left( v'_r, \sqrt{\frac{2}{2-s}} v'_\theta, v'_z \right), \quad (8)$$

$$p' \mapsto h \equiv \frac{\sqrt{r}}{\sqrt{\rho_0} c_s} p', \quad (9)$$

where  $s \equiv \frac{d \ln \Omega}{d \ln r}$ . It reveals a symmetrized set of equations, which simplifies the subsequent choice of

inner product introduced for the topological analysis (Leclerc et al. 2022, see Sect. 2.2). Performing a Fourier transform  $e^{i\omega t - ik_z z}$  yields a wave equation for  $X^\top \equiv (u_z \ u_r \ u_\theta \ h)^\top$  of the form

$$\mathcal{H}X = \omega X, \quad (10)$$

$$\mathcal{H} = \quad (11)$$

$$\begin{pmatrix} 0 & 0 & 0 & c_s k_z \\ 0 & 0 & -i\kappa & ic_s \partial_r + \frac{i}{2} \frac{dc_s}{dr} - iS \\ 0 & i\kappa & 0 & 0 \\ c_s k_z & ic_s \partial_r + \frac{i}{2} \frac{dc_s}{dr} + iS & 0 & 0 \end{pmatrix},$$

where  $\kappa \equiv \sqrt{2(2-s)}\Omega$  is the epicyclic frequency and

$$S \equiv \frac{c_s}{2} \left( \frac{d \ln p_0}{dr} + \frac{d \ln c_s}{dr} + \frac{1}{r} \right) \quad (12)$$

denotes the *epicyclic-acoustic frequency* of the disc, acting as a cutoff frequency as we will show in the local dispersion relation. To the best of our knowledge, this is the first explicit identification of the frequency that governs momentum exchange between the inertial and acoustic bands in discs. Its expression follows directly from the rescaled symmetric Hermitian formulation of the wave equations.  $S$  depends on the radial inhomogeneity and the curvature of the disc. Terms associated to Eq. (12) break the symmetry  $(r, u_r, u_\theta) \rightarrow -(r, u_r, u_\theta)$ , which is only restored when  $S = 0$ .  $S$  plays the role, in discs, of the buoyant-acoustic frequency identified in stars by (Leclerc et al. 2022). For a stratified disc, this expression can be conveniently rewritten

$$S = \frac{1}{2} \left[ \frac{d \ln p_0}{d \ln r} + \frac{d \ln c_s}{d \ln r} + 1 \right] \frac{H_P}{r} \Omega, \quad (13)$$

where  $H_P \equiv c_s \Omega^{-1}$  is the pressure scale height of the disc.

We impose impenetrable boundaries, such that  $u_r(r_0) = u_r(r_1) = 0$ . For real  $\kappa$  (a Rayleigh stable disc), the operator  $\mathcal{H}$  is self-adjoint with respect to the canonical inner product  $\langle X, Y \rangle = \int dr X^\dagger Y$ . The frequencies  $\omega$  are then guaranteed to be real: the perturbations considered here are linearly stable. The self-adjointness of  $\mathcal{H}$  gives the following energetic constant of motion

$$I = \frac{1}{2} \langle X, X \rangle, \quad (14)$$

$$= \int dr \frac{1}{2} (|u|^2 + |h|^2), \quad (15)$$

$$= \int dr r \left[ \frac{1}{2} \rho \left( |v'_r|^2 + \frac{2}{2-s} |v'_\theta|^2 + |v'_z|^2 \right) + \frac{1}{2\rho c_s^2} |p'|^2 \right],$$

(see Appendices for a proof). The solutions to Eqs.(10)-(11), together with these boundary conditions, are the axisymmetric oscillation modes of the disc, i.e. the standing waves in the radial direction.

## 2.2. Local wave equation

Microlocal analysis is a representation of differential operators on a phase space using the Wigner transform (Keppeler 2004; Hall 2013). This transform maps (pseudo-)differential operators to *symbols*, i.e functions of the phase space. Three useful symbols used here are

$$\text{Symb}[c_s(r)] = c_s, \quad (16)$$

$$\text{Symb}[i\partial_r] = k_r, \quad (17)$$

$$\text{Symb}[ic_s \partial_r + \frac{i}{2} \frac{dc_s}{dr}] = c_s k_r. \quad (18)$$

It gives an appropriate way to define a local wavenumber  $k_r$  for a wave (Onuki 2020).

The operator  $\mathcal{H}$  is then mapped to its symbol  $H$

$$H = \begin{pmatrix} 0 & 0 & 0 & c_s k_z \\ 0 & 0 & -i\kappa & c_s k_r - iS \\ 0 & i\kappa & 0 & 0 \\ c_s k_z & c_s k_r + iS & 0 & 0 \end{pmatrix}. \quad (19)$$

The Wigner transform has a number of useful properties, among which is the conservation of Hermiticity:  $\mathcal{H}$  is a self-adjoint differential operator if and only if  $H$  is a Hermitian matrix function (one can find this property in (Hall 2013), page 266). It is then guaranteed that  $H$  gives the local dispersion relation of the waves without introducing spurious instabilities, as it has been shown to happen when including pressure gradients in local studies (e.g. see discussions in Lin and Youdin 2015; Latter and Papaloizou 2017). Indeed, one has  $H^\dagger = H$ . The local wave equation is

$$HX = \omega X, \quad (20)$$

and the local dispersion relation is simply obtained by  $\det(H - \omega \mathbf{1}) = 0$ , which yields

$$c_s^2 k_r^2 = \frac{(c_s^2 k_z^2 - \omega^2)(\kappa^2 - \omega^2)}{\omega^2} - S^2. \quad (21)$$

Equation (21) is a quadratic polynomial in  $\omega^2$ , whose smaller root corresponds to the inertial band (or  $r$ -band) and the larger to the pressure band (or  $p$ -band). For inertial waves, one has  $0 \leq \omega^2 \leq \kappa^2$ , while for pressure waves,  $\omega^2 \geq \kappa^2 + S^2$ . Thus, a nonzero value of  $S$  opens a frequency gap between the bands, and no wave with  $\omega^2 \in (\kappa^2, \kappa^2 + S^2)$  can propagate radially in the disc. The dispersion relation derived by other local expansions, which neglect both the curvature term and the pressure gradient, is recovered for  $S = 0$ . In that special case, there is a degeneracy between acoustic and inertial waves at  $\omega = \kappa$  for  $(k_r, k_z) = (0, \kappa/c_s)$ , but it is lifted by any nonzero value of  $S$ , i.e any nonzero pressure gradient or by the curvature term.

### 3. TOPOLOGY AND GLOBAL MODES

#### 3.1. Chern numbers

The symbol  $H$  obtained from the microlocal analysis formally coincides with that derived for stellar oscillations in [Leclerc et al. \(2022\)](#), who demonstrated that these degeneracies in the local dispersion relation are linked to topological charges known as Chern numbers ([Volovik 2003](#); [Delplace 2022](#)). According to the principle called index theorem, this implies the presence of a spectral flow in the dispersion relation of the global modes  $\{\omega_n\}_{n \in \mathbb{N}}$  ([Delplace et al. 2017](#); [Delplace 2022](#); [Faure 2023](#)). A spectral flow is the fact that a finite number of modes branches transit from one band to the other as the parameter  $k_z$  increases, in that case between the band of  $r$ -modes and the band of  $p$ -modes. This number of branches precisely equals a topological index of the symbol called the first Chern number.

Following [Leclerc et al. \(2022\)](#), we define and compute the Chern numbers for the wavebands in the disc. For a given eigenvector  $X$  of a given band of  $H$  (either the  $r$ - or the  $p$ - band), the Berry curvature is the vector field in the parameter space  $(k_r, S, k_z)$  expressed as

$$\mathbf{F} = i \nabla \times (X \cdot \nabla X), \quad (22)$$

where  $\nabla = (\partial_{k_r}, \partial_S, \partial_{k_z})$ . This convenient expression only holds in a 3D parameter space, although more general definitions exist ([Delplace 2022](#)).  $\mathbf{F}$  is singular when frequencies degenerate, which occurs for  $k_r = S = 0$  and  $c_s k_z = \pm \kappa$ . Fig. 1 displays  $\mathbf{F}$  for the acoustic wave, revealing the two singularities associated with the degeneracies.

The Chern number characterizes these singularities. It is an integer defined as

$$\mathcal{C} = \frac{1}{2\pi} \oint_{\Sigma} \mathbf{F} \cdot d\mathbf{\Sigma}, \quad (23)$$

where  $\Sigma$  is any closed surface enclosing one singularity. Numerical computations show that the two degeneracies at  $k_r = S = 0$  and  $c_s k_z = \pm \kappa$  have Chern numbers

$$\mathcal{C} = \pm 1. \quad (24)$$

These values are expected from the formal analogy with the problem of [Leclerc et al. \(2022\)](#).

The Chern number is computed in the local analysis; however, it has direct consequences on the global waves by imposing a spectral flow, the existence of modes whose frequencies approach both wavebands (inertial and acoustic) for different limits of  $k_z$ . The non-zero Chern numbers calculated by [Leclerc et al. \(2022\)](#) impose the propagation of a Lamb-like wave in non-rotating stars crossing the frequency gap between acoustic and internal gravity waves ([Perrot et al. 2019](#); [Leclerc](#)

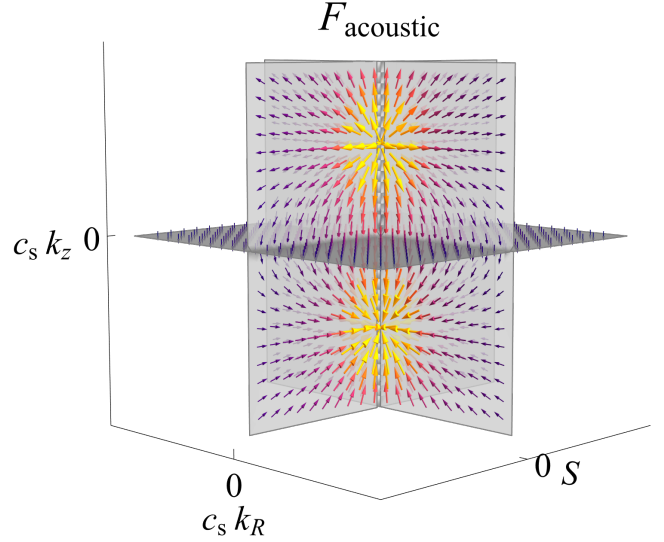


**Figure 1.** The Berry curvature  $\mathbf{F}$  of the acoustic wave is singular at  $(c_s k_r, S, c_s k_z) = (0, 0, \pm \kappa)$ . This obstruction is a topological constraint, characterized by the two charges  $\mathcal{C} = \pm 1$ . Length and brightness of the arrows indicate the norm of  $\mathbf{F}$ .

[et al. 2022](#)). We then expect to have one global wave branch with such spectral behavior in the spectrum of a disc.

#### 3.2. Location of topological modes

The spatial location of topological modes corresponding to the spectral flow branch is determined by whether a radius exists where

$$S = 0, \quad (25)$$

as it is the point where the topological degeneracy occurs in Fig. 1. If such a topological interface is present in the disc, the energy of the modes are concentrated in a volume centered around this interface over a typical radial length  $\mathcal{L}$  given by

$$\mathcal{L} \equiv \sqrt{c_s / \left| \frac{dS}{dr} \right|_{S=0}}. \quad (26)$$

The steeper  $S$  is near the topological interface, the more tightly confined the topological modes are. If  $S$  has a constant sign throughout the object, the modes are located at one of the boundaries: at the inner edge if  $S < 0$  and at the outer edge if  $S > 0$  (See the discussion of [Iga 2001](#), page 483 for a similar result in an atmospheric context). This behavior is a manifestation of the general bulk-boundary correspondence known in condensed matter physics: the topological properties of a material, calculated in the bulk of the domain, determine the existence and nature of some modes that appear at its boundaries ([Delplace 2022](#)).



### 3.3. Monotonic disc profiles

We first consider a disc whose density, temperature and rotation rate are parametrized by typical power-laws (Armitage 2011). More precisely, the temperature scales as  $T(r) \propto r^{-q}$ , the surface density as  $\Sigma(r) \propto r^{-p}$  and the rotation rate as  $\Omega(r) \propto r^{-s}$ . Hence, volume density scales as  $\rho \propto \frac{\Omega}{c_s} \Sigma \propto r^{-p-s+\frac{q}{2}}$  and

$$S = \frac{1}{2} [1 - p - q - s] \frac{H}{r} \Omega. \quad (27)$$

For physically realistic profiles,  $1 - p - q - s < 0$  and thus  $S < 0$  throughout the disc. As discussed in Sect. 3.2, a topological mode is expected to be located at the inner edge of the disc.

We verify this prediction by solving Eqs. (10)-(11) numerically using the EVP class of the DEDALUS python package (Burns et al. 2020; Oishi et al. 2021). The gas is contained between two radii  $r_0$  and  $r_1 = 10r_0$ . Units of lengths and time are  $r_0$  and  $\Omega(r_0)^{-1}$  and the dimensionless parameters are  $p = 1$ ,  $q = \frac{1}{2}$ ,  $s = \frac{3}{2}$  and  $\frac{c_s}{R\Omega}|_{r_0} = 0.1$ . Figure 2 shows the density profile of the disc and the frequencies of the global waves for a range of vertical wavenumbers  $k_z$ . The average energy-weighted position  $\langle r \rangle \equiv \langle X, rX \rangle / \langle X, X \rangle$  for a mode  $X(r)$  is provided via the color bar. Low frequency  $p$ -modes are located mostly in the outer parts of the disc, where the sound speed is the lowest. High frequency  $r$ -modes are located mostly in the inner part, where the epicyclic frequency  $\kappa$  is maximal. Due to these spatial variations, the two bands of frequency of these two families of modes superimpose significantly, but separate asymptotically at  $k_z \rightarrow 0$  and  $k_z \rightarrow \infty$ . Indeed, at low  $k_z$ , acoustic modes reach non-zero frequencies, while inertial waves all have zero frequency. On the other hand at large  $k_z$ , the inertial wave reach finite frequencies, while the acoustic waves follow  $\omega \propto k_z$ .

One mode falls outside this classification: it reaches zero frequency as  $k_z \rightarrow 0$ , yet behaves as  $\omega \propto k_z$  for large  $k_z$ . This mode corresponds to the spectral flow: as  $k_z$  increases, its branch transits from the inertial waveband to the acoustic waveband. Numerical integration shows that this branch corresponds to the fundamental modes of the disc, which have no radial node of pressure or vertical velocity. It follows the dispersion relation  $\omega = c_s(r_0)k_z$  (grey thin line on Fig. 2), as it is indeed located at the inner boundary  $r_0$ , and is acoustic in nature.

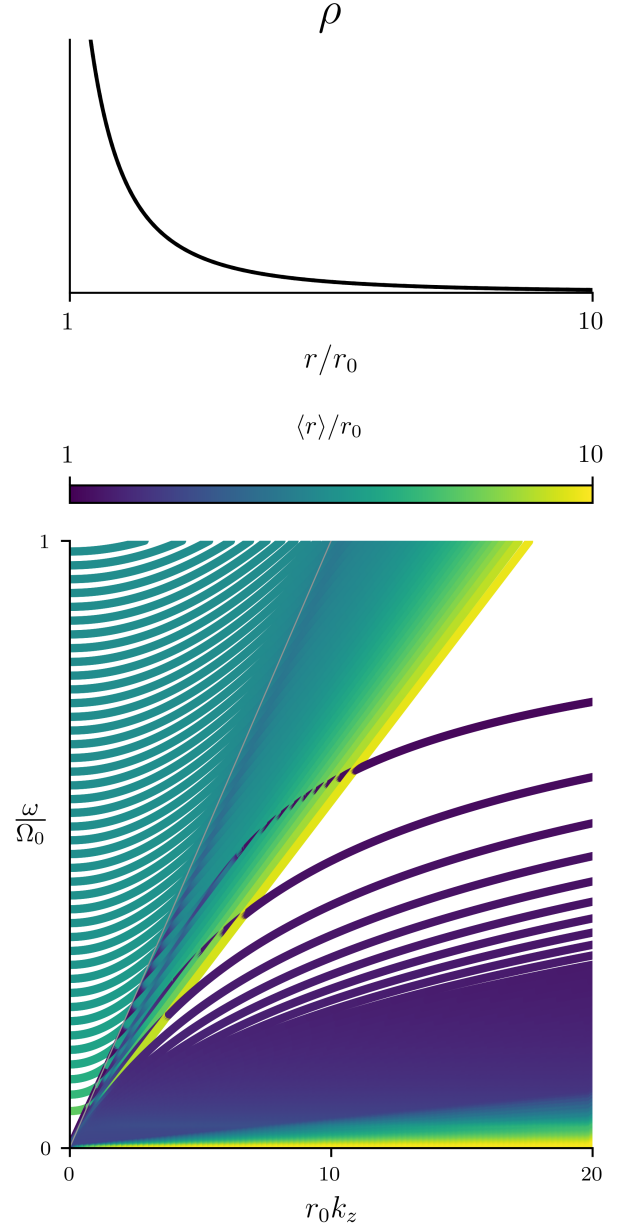


**Figure 2.** Global modes of a monotonic disc. The one topological branch transits from inertial modes (blue) at low  $k_z$  to acoustic modes (yellow) at high  $k_z$ . It matches the dispersion relation  $\omega = c_s(r_0)k_z$  (grey thin line).

## 4. PRESSURE EXTREMA

### 4.1. Slender tori

Singularities of Berry curvature occur when  $S = 0$ . Interestingly, when the spatial curvature term is negligible in Eq. (13), this coincides with local pressure extrema, which occur in structured discs in the form of rings and gaps (Andrews et al. 2018). One therefore expects topological modes to propagate around pressure maxima and

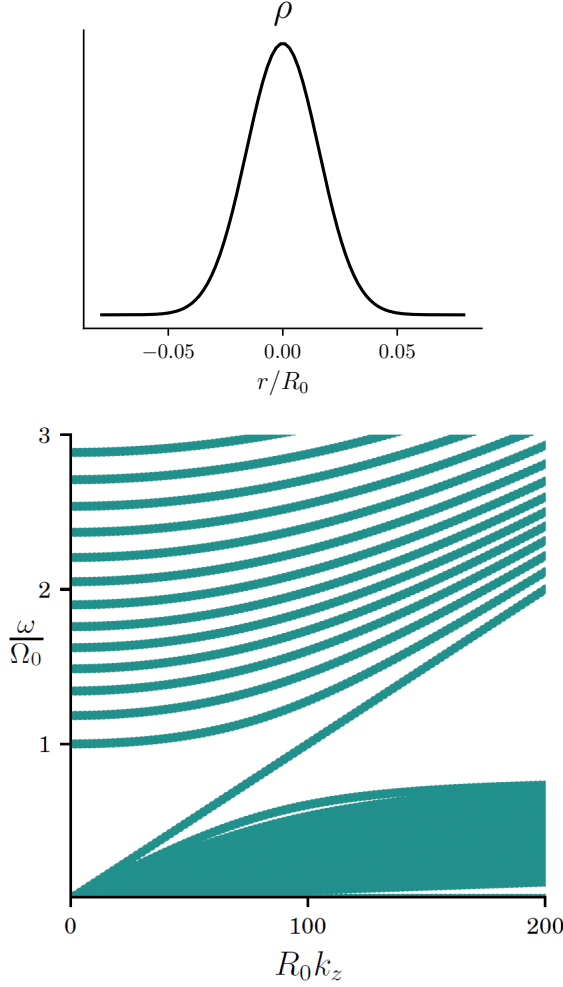


**Figure 3.** Dispersion relations of the global modes in a slender torus.

minima. To investigate this expectation, we study the isothermal slender torus model (Papaloizou and Pringle 1985), a model of rings in which the radial extent of the gas is assumed to be small compared to the distance to the star  $r$ , thereby enforcing strong radial pressure gradients. The gas density of the slender torus is parametrized by

$$\rho_0(r) = \rho_c \exp\left(-\frac{(r - r_0)^2}{2L^2}\right), \quad (28)$$

$$S(r) = -\frac{c_s}{2L^2}(r - r_0), \quad (29)$$

where here  $r_0$  is the position of the pressure maximum,  $L^2 = \frac{c_s^2 \Omega_0^{-2}}{(2s-3)}$ , with  $s = \frac{d \ln \Omega}{d \ln r}$  and  $\Omega_0 = \Omega(r_0)$ .  $S$  vanishes at  $r = r_0$ , which implies that the topological mode is trapped around this position.

Since  $S$  varies linearly with  $r$ , analytical solutions for global modes can be found (a similar solution has been

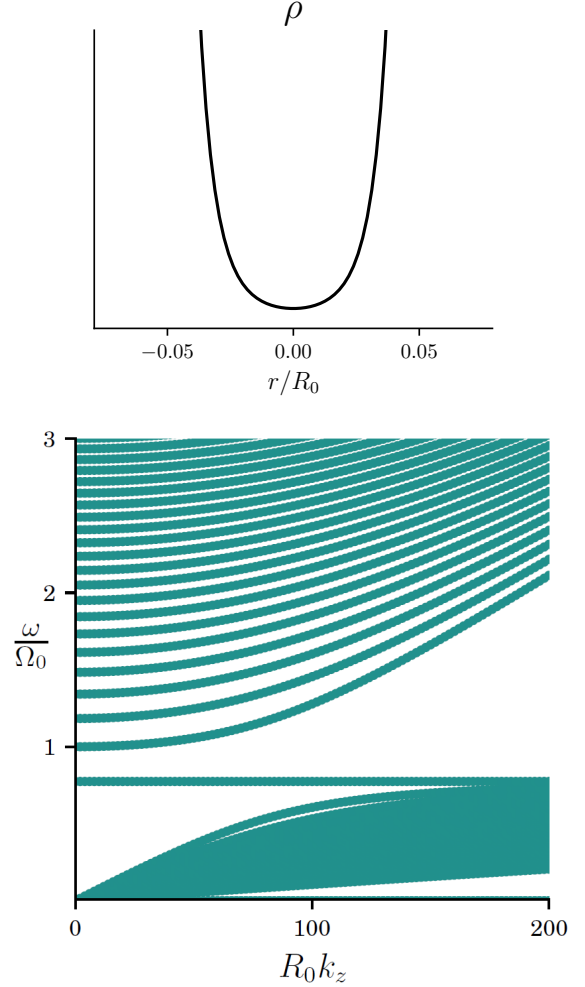


**Figure 4.** Dispersion relations of the global modes in a pressure minimum.

derived for stars in Leclerc et al. 2022). For an isothermal disc, eliminating  $u_\theta$  and  $u_z$  in Eq. (10), it can then be written in the compact form

$$u_r = \left(\omega - \frac{\kappa^2}{\omega}\right)^{-1} \mathcal{D}h, \quad (30)$$

$$\mathcal{D}^\dagger \mathcal{D}h = \lambda h, \quad (31)$$

where  $\mathcal{D} \equiv ic_s \partial_r - iS(r)$  and  $\lambda \equiv \left(\omega - \frac{\kappa^2}{\omega}\right) \left(\omega - \frac{c_s^2 k_z^2}{\omega}\right)$ . The slender torus model verifies Eq. (29) and as such, the global modes equation Eq. (31) reads

$$\left(-\partial_{rr} + \frac{(r - r_0)^2}{4L^4} - \frac{1}{2L^2} - \frac{\lambda}{c_s^2}\right) h = 0, \quad (32)$$

which is the differential eigenvalue equation of the Quantum Harmonic Oscillator (Abramowitz and Stegun 1972). Imposing regularity at infinity, the solutions of Eq. (32) are Hermite polynomials  $H_n$  with associated

frequencies  $\omega_n$ , so that the normal modes of the disc are

$$p'/\rho_0 \propto v'_z \propto H_n \left( \frac{r-r_0}{\sqrt{2}L} \right), \quad (33)$$

$$v'_r \propto v'_\theta \propto \sqrt{n} H_{n-1} \left( \frac{r-r_0}{\sqrt{2}L} \right), \quad (34)$$

$$\frac{n}{L^2} = \frac{(c_s^2 k_z^2 - \omega_n^2)(\kappa_c^2 - \omega_n^2)}{c_s^2 \omega_n^2}. \quad (35)$$

In the solutions,  $n$  is a non-negative integer that corresponds to the number of radial nodes in the pressure perturbation profile. For  $n \geq 1$ , two modes satisfy Eq. (35): one acoustic and one inertial, both of radial order  $n$ . For  $n = 0$ , only a single solution with finite kinetic energy exists (for which  $v'_r = v'_\theta = 0$ ), namely

$$\omega_{n=0} = \pm c_s k_z. \quad (36)$$

This mode propagates at all frequencies and as such, transits between the frequency bands. This mode and its behavior among the rest of the spectrum of the slender torus are shown on Fig. 3.

#### 4.2. Pressure minima

Interestingly, the topological arguments also suggests modes trapped at a pressure minima. We therefore study a model of a gap given by the inverse of the slender torus profile, parametrized by

$$\rho_0(r) = \rho_c \exp \left( + \frac{(r-r_0)^2}{2L^2} \right), \quad (37)$$

$$S(r) = + \frac{c_s}{2L^2} (r-r_0). \quad (38)$$

While  $S$  passes through zero with a negative slope at pressure maxima, at pressure minima this slope is instead positive. Nevertheless, the differential equation Eq.(11) differs very little, and the solutions of this model read

$$p'/\rho_0 \propto v'_z \propto \sqrt{n} \exp \left( - \frac{(r-r_0)^2}{2L^2} \right) H_{n-1} \left( \frac{r-r_0}{\sqrt{2}L} \right) \quad (39)$$

$$v'_r \propto v'_\theta \propto \exp \left( - \frac{(r-r_0)^2}{2L^2} \right) H_n \left( \frac{r-r_0}{\sqrt{2}L} \right), \quad (40)$$

$$\frac{n}{L^2} = \frac{(c_s^2 k_z^2 - \omega_n^2)(\kappa_c^2 - \omega_n^2)}{c_s^2 \omega_n^2}. \quad (41)$$

Again, in this set of solutions, the  $n = 0$  case only has one solution with finite kinetic energy, which is the mode with constant frequency

$$\omega = \pm \kappa \quad (42)$$

This mode is a spectral flow *in the other direction* than at a pressure maximum, since the branch transits from the acoustic band to the inertial band as  $k_z$  increases, and is shown in Fig. 4.

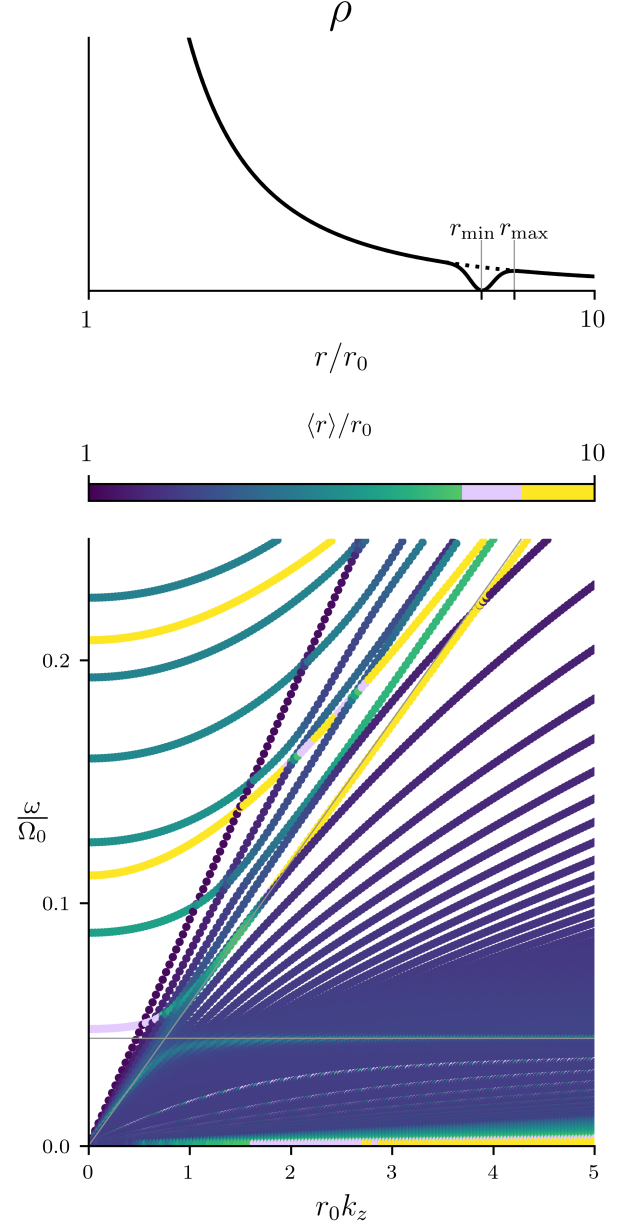


**Figure 5.** Same as Fig. 2, for a disc with a gap and zoomed on lower frequencies. In a disc where a gap of density is present, one local minimum and one local maximum of density are found. Associated to these extrema, two topological modes are expected and found in the spectrum, one inertial and one acoustic respectively. Grey lines:  $\omega = \kappa(r = r_{\min})$  and  $\omega = c_s(r = r_{\max})k_z$ .

#### 4.3. Gap in a disc

In order to test these predictions in a realistic gap in a disc, we study the spectrum of an extended disc with power-law profiles as discussed in Sec. 3.3, on top of which is carved a gap. More precisely, volume density

is taken as

$$\rho \propto r^{-p-s+\frac{q}{2}} \times (1 - A \exp(-(r - r_{\text{gap}})^2 / 2L_{\text{gap}}^2)). \quad (43)$$

This profile is shown on Fig. 5 (top), with the position of the gap  $r_{\text{gap}} = 8r_0$ , width of the gap  $L_{\text{gap}} = 0.2r_0$  and relative depth of the gap  $A = 0.99$ .

Interestingly, the addition of a gap in the disc causes the addition of two new extrema of density: a minimum and a maximum, separated by approximately half the gap width. By the analysis described in the sections above, one expects two topological modes localized at these regions of the disc, trapped by the density extrema. Close to  $r_{\text{min}}$  and therefore close to the center of the gap, one expects an epicyclic mode with dispersion relation  $\omega = \kappa(r = r_{\text{min}})$ , and an acoustic mode close to  $r_{\text{max}}$  with dispersion relation  $\omega = c_s(r = r_{\text{max}})k_z$ .

The bottom panel of Fig. 5 presents the numerically obtained spectrum of the disc. As before, the colors indicate the average mode positions, with modes located inside the gap highlighted in pink.

In addition to the inertial and acoustic branches already present in the monotonic disc, one observes a new set of inertial branches (low-frequency, pink) as well as a new set of acoustic branches (yellow). Moreover, the two branches of modes predicted by the topological analysis are also visible, with their dispersion relations overlaid as thin grey lines. An inertial branch appears at  $\omega = \kappa(r = r_{\text{min}})$ , while an acoustic branch follows  $\omega = c_s(r = r_{\text{max}})k_z$ . Because these two modes occupy nearby regions in radius, they hybridize when their frequencies align, leading to an avoided crossing near  $r_0 k_z \sim 0.8$ . The low-frequency pink branch is not incidental: it represents a mode trapped in the gap and corresponds to the topological epicyclic mode, as evidenced by its eigenfunctions (see Appendix C).

Therefore, the density extrema act as waveguides, trapping modes in the way described in the analytical models presented in Sect. 4.1 and 4.2. In addition to the two topological modes, new branches of inertial modes appeared in the spectrum at low frequency, trapped in the gap. New branches of acoustic modes appear with average position in the yellow region, as those are instead trapped between the gap and the outer boundary. In that case, it appears that the gap of the disc acts as a reflector for acoustic waves.

## 5. DISCUSSION

By leveraging topological methods, our analysis characterizes how large-scale modes behave in radially structured discs. Emphasis was put on the role that radial pressure and density gradients play on linear stable

waves, encapsulated by the characteristic frequency  $S$ . Using microlocal techniques, we show that these gradients modify the local dispersion relations by coupling acoustic and inertial waves and removing their frequency degeneracy. As such,  $S$  naturally acts as a cutoff frequency and offers a consistent way to account for gradient effects in local analyses. Topological arguments highlight the significance of points where  $S = 0$ , which carry topological charges (Chern numbers  $\mathcal{C} = \pm 1$ ). These charges enforce the emergence of modes with unique spectral properties, namely branches that transit between  $r$ -modes and  $p$ -modes. While a monotonic disc hosts only one such branch, structured discs contain additional ones, as illustrated in Fig. 5. We emphasize that the gapped-disc model presented in Sect. 4.3 is intended as an illustrative example of trapped modes; although it reproduces the expected topological modes at pressure extrema, it is not meant to be realistic or to remain stable against the Rossby wave instability (Lovelace et al. 1999).

The fundamental mode trapped at a pressure maximum propagates for all frequencies and is the sole mode to do so (see Fig. 3), making it capable of resonating with any temporal forcing, unlike modes with forbidden frequency domains. It is a vertical acoustic wave (see Figs. 6-7). By contrast, the fundamental mode associated with a pressure minimum (a gap) propagates only at the constant frequency  $\omega = \kappa$  (see Fig. 4 and Figs. 8-9), and is a horizontal, epicyclic wave. This unique property thereby allows for a propagation at arbitrary vertical phase velocities. Indeed, since  $\frac{\omega}{k_z} = \frac{\kappa}{k_z}$  can take any value, this mode is unique among the modes in having an arbitrary vertical phase velocity. This is a necessary condition for resonating with any vertical dust flow involved in dust-settling instabilities, a class of resonant drag instabilities (e.g. Squire and Hopkins 2018; Zhuravlev 2019; Lehmann and Lin 2023; Paardekooper and Aly 2025). In the analytical model of Sec. 4.2, this mode has no vertical velocity and therefore does not couple to vertical flows *a priori*. However, we emphasize that this is a peculiarity of that model. In general, the mode does exhibit some vertical-velocity perturbation (see Appendix C): this topological mode may thus couple to vertical flows in settling-instability mechanisms. It would be worthwhile to further investigate its role at the outer edge of a planetary gap, where dust accumulates.

The spectrum of a disc with a pressure bump instead of a pressure gap produces similar results (see Fig. 10).



At low  $k_z$  (see Figure 8) this mode exhibits a very similar character to the trapped  $r$ -modes found in black hole accretion discs (Kato 2004, 2008; Ferreira and Ogilvie 2008; Dewberry et al. 2018). Only here the mode is confined by the epicyclic-acoustic frequency rather than by the maximum in the relativistic epicyclic frequency found in black hole discs. This leaves open the possibility that this mode could be excited to large amplitudes via a similar three-wave coupling mechanism (Kato 2004, 2008; Ferreira and Ogilvie 2008), where the  $r$ -mode is coupled to a global  $m = 1$  deformation in such a way that it leads to growth in the  $r$ -mode amplitude. Candidates for such a global  $m = 1$  deformation include remnant disc eccentricity left over from the disc formation process (Commerçon et al. 2024), or disc warping and eccentricity excited by an embedded planet (Lubow and Ogilvie 2001; Teyssandier and Ogilvie 2016).

The main limitations of the present study are the absence of vertical stratification and of any linear instability. The vertical stratification is sometimes separated from the radial problem by averaging vertically (e.g. Papaloizou and Pringle 1985 or Blaes et al. 2006); we instead chose to assume no stratification, in order to keep the notion of a vertical wavenumber  $k_z$ . We note that our analytical solutions for the slender torus Eq. (35) matches those of Blaes et al. (2006), see their Eq. 56 for their  $n$  set to  $\infty$  and our  $k_z = 0$ .

We also note that Eq. (21) is analogous to the one found by Okazaki et al. 1987 (Eq. 4.4) who studied vertical isothermal stratification and no radial stratification, with two expected differences: the addition of  $S^2$  representing radial gradients in our case, and the replacement of  $c_s^2 k_z^2$  by  $n_z \kappa^2$  in their case, where  $n_z$  is a positive integer counting the number of nodes in the profile of pressure perturbation given by the Hermite function of order  $n_z$ . Thus, vertical isothermal stratification seems to be fully taken into account by discretizing wavenumbers as  $c_s k_z = n_z^{1/2} \kappa$ . However, the results of Korycansky and Pringle 1995 suggest an interesting behavior of the modes with vertical stratification and no radial gradients (see their Fig.1). Indeed, they show that a pair of fundamental  $p$ -modes with indices  $n_z = 0, 1$  have frequencies connecting inertial modes and acoustic modes, possibly performing a spectral flow. This suggests that, complementarily, vertical stratification imposes another set of topological properties and topological modes, regardless of radial gradients.

The analytical techniques and solutions found for modes of non-axisymmetric polytropic discs, slender (Papaloizou and Pringle 1985; Blaes 1985; Blaes et al. 2006) or thick (Blaes et al. 2007) provide the support to ex-

plore the topology of these waves rising from vertical inhomogeneity, and from azimuthal wavenumbers, and possibly associated topological modes. Our goal in the present study is to provide a starting point for applying topological analysis to linear waves in discs, a framework whose predictive power can yield new insights into large-scale oscillations in inhomogeneous discs, with the perspective of establishing robust and possibly unique properties of large-scale modes falling out of WKB approaches. This line of research is motivated by the anticipated potential of discoseismology in protoplanetary discs, facilitated by line-kinematic measurements from ALMA (e.g. Pinte et al. 2023; Teague et al. 2025). While this perspective is still far off, we expect that the spatial patterns of the eigenmodes may provide constraints on models—a key distinction from stellar pulsation studies. The employment of topological analysis to study linear instabilities in discs requires further investigation, as it is a field of research less developed than topology of stable waves. In stellar context, these ideas have led to the unveiling of fast-growing large-scale modes of compressible convective instability (Leclerc et al. 2024a). Similar results may be expected in discs instabilities, when accounting for the role of pressure gradients as we did in the present study.

## 6. CONCLUSION

Motivated by the foreseen potential of discoseismology in protoplanetary discs enabled by line-kinematic measurements from ALMA, we conduct a topological analysis of radial waves in unstratified astrophysical discs. The main conclusions are:

1. **Existence of robust topological modes :** Global large-scale modes transiting between the inertial and the acoustic bands exist in discs. These modes find their roots in topological numbers, and as such qualify as being *topological modes*. This special origin provides them with unique properties.
2. **Epicyclic-acoustic frequency :** The existence of topological modes in discs is associated with the cancellation of the *epicyclic-acoustic* frequency  $S$  given by Eq. 12, which gives the rate of momentum exchange between the inertial and acoustic bands. This is why monotonic-density discs support a single topological mode at their inner edge.
3. **Role of pressure extrema :** Pressure maxima and minima, acting as waveguides, generate additional topological modes because  $S = 0$  at these locations. The associated topological branch is

acoustic at pressure maxima and inertial at pressure minima, both having unique specificity across the spectrum (any frequency or any phase velocity). Their distinct features make them appealing targets for future line-based discoseismology. Furthermore, they are potentially easier to detect as they are localized, and their radial trapping would provide a direct measure of the pressure gradient of the bump/dip.

4. **Microlocal framework** : The microlocal analysis introduced here enables the study of local wave properties without using a shearing box, while preserving the Hermitian structure of the problem. This approach provides a powerful framework for studying linear modes in discs.

As commented on in the discussion, we focused on the midplane, ignoring for the moment the influence of

vertical stratification. Treating simultaneously vertical and radial gradients requires a complementary study, which may reveal additional topological structures in the higher-dimensional parameter space involved. A stepping stone towards general results and potentially discoseismology is to study a dual simplified problem where radial gradients are neglected while keeping vertical stratification. A study focusing on the topological modes of this problem will be the object of a future work.

## ACKNOWLEDGEMENTS

AL was funded by Contrat Doctoral Spécifique Normaliens during this work. GL, EL and NP acknowledge funding from ERC CoG project PODCAST No 864965. We used MATHEMATICA (Wolfram Research, Inc. 2024). The scripts used for numerical calculations are accessible at <https://github.com/ArmandLeclerc/radialStratifDisc>.

## REFERENCES

- V. S. Safronov. *Evolution of the protoplanetary cloud and formation of the earth and planets*. 1972.
- J. Bae, A. Isella, Z. Zhu, R. Martin, S. Okuzumi, and S. Suriano. Structured Distributions of Gas and Solids in Protoplanetary Disks. In S. Inutsuka, Y. Aikawa, T. Muto, K. Tomida, and M. Tamura, editors, *Protostars and Planets VII*, volume 534 of *Astronomical Society of the Pacific Conference Series*, page 423, July 2023. <https://doi.org/10.48550/arXiv.2210.13314>.
- G. Lesur, M. Flock, B. Ercolano, M. K. Lin, C. Yang, J. A. Barranco, P. Benitez-Llambay, J. Goodman, A. Johansen, H. Klahr, G. Laibe, W. Lyra, P. S. Marcus, R. P. Nelson, J. Squire, J. B. Simon, N. J. Turner, O. M. Umurhan, and A. N. Youdin. Hydro-, Magnetohydro-, and Dust-Gas Dynamics of Protoplanetary Disks. In S. Inutsuka, Y. Aikawa, T. Muto, K. Tomida, and M. Tamura, editors, *Protostars and Planets VII*, volume 534 of *Astronomical Society of the Pacific Conference Series*, page 465, July 2023. <https://doi.org/10.48550/arXiv.2203.09821>.
- J. Drazkowska, B. Bitsch, M. Lambrechts, G. D. Mulders, D. Harsono, A. Vazan, B. Liu, C. W. Ormel, K. Kretke, and A. Morbidelli. Planet Formation Theory in the Era of ALMA and Kepler: from Pebbles to Exoplanets. In S. Inutsuka, Y. Aikawa, T. Muto, K. Tomida, and M. Tamura, editors, *Protostars and Planets VII*, volume 534 of *Astronomical Society of the Pacific Conference Series*, page 717, July 2023. <https://doi.org/10.48550/arXiv.2203.09759>.
- C. Pinte, R. Teague, K. Flaherty, C. Hall, S. Facchini, and S. Casassus. Kinematic Structures in Planet-Forming Disks. In S. Inutsuka, Y. Aikawa, T. Muto, K. Tomida, and M. Tamura, editors, *Protostars and Planets VII*, volume 534 of *Astronomical Society of the Pacific Conference Series*, page 645, July 2023. <https://doi.org/10.48550/arXiv.2203.09528>.
- Richard Teague, Myriam Benisty, Stefano Facchini, Misato Fukagawa, Christophe Pinte, Sean M. Andrews, Jaehan Bae, Marcelo Barraza-Alfaro, Gianni Cataldi, Nicolás Cuello, Pietro Curone, Ian Czekala, Daniele Fasano, Mario Flock, Maria Galloway-Sprietsma, Himanshi Garg, Cassandra Hall, Iain Hammond, Thomas Hilder, Jane Huang, John D. Ilee, Andrés F. Izquierdo, Kazuhiro Kanagawa, Geoffroy Lesur, Giuseppe Lodato, Cristiano Longarini, Ryan A. Loomis, Frédéric Masset, Francois Menard, Ryuta Orihara, Daniel J. Price, Giovanni Rosotti, Jochen Stadler, Leonardo Testi, Hsi-Wei Yen, Gaylor Wafflard-Fernandez, David J. Wilner, Andrew J. Winter, Lisa Wölfer, Tomohiro C. Yoshida, and Brianna Zawadzki. exoALMA. I. Science Goals, Project Design, and Data Products. *ApJL*, 984(1):L6, May 2025. <https://doi.org/10.3847/2041-8213/adc43b>.

- J. E. Solheim, J. L. Provencal, P. A. Bradley, G. Vauclair, M. A. Barstow, S. O. Kepler, G. Fontaine, A. D. Grauer, D. E. Winget, T. M. K. Marar, E. M. Leibowitz, P. I. Emanuelson, M. Chevreton, N. Dolez, A. Kanaan, P. Bergeron, C. F. Claver, J. C. Clemens, S. J. Kleinman, B. P. Hine, S. Seetha, B. N. Ashoka, T. Mazeh, A. E. Sansom, R. W. Tweedy, E. G. Meistas, A. Bruvold, and C. M. Massacand. Whole Earth Telescope observations of AM Canum Venaticorum - discoseismology at last. *A&A*, 332:939–957, April 1998.
- David Tsang and Dong Lai. Corotational damping of discoseismic c modes in black hole accretion discs. *MNRAS*, 393(3):992–998, March 2009. <https://doi.org/10.1111/j.1365-2966.2008.14228.x>.
- David Tsang and Iryna Butsky. Iron line variability of discoseismic corrugation modes. *MNRAS*, 435(1):749–765, October 2013. <https://doi.org/10.1093/mnras/stt1334>.
- M. Ortega-Rodríguez, H. Solís-Sánchez, L. Álvarez-García, and E. Doderó-Rojas. On twin peak quasi-periodic oscillations resulting from the interaction between discoseismic modes and turbulence in accretion discs around black holes. *MNRAS*, 492(2):1755–1760, February 2020. <https://doi.org/10.1093/mnras/stz3541>.
- Janosz W. Dewberry, Henrik N. Latter, Gordon I. Ogilvie, and Sebastien Fromang. HFQPOs and discoseismic mode excitation in eccentric, relativistic discs. I. Hydrodynamic simulations. *MNRAS*, 497(1):435–450, September 2020a. <https://doi.org/10.1093/mnras/staa1897>.
- Janosz W. Dewberry, Henrik N. Latter, Gordon I. Ogilvie, and Sebastien Fromang. HFQPOs and discoseismic mode excitation in eccentric, relativistic discs. II. Magnetohydrodynamic simulations. *MNRAS*, 497(1):451–465, September 2020b. <https://doi.org/10.1093/mnras/staa1898>.
- Shoji Kato. Damping of disco-seismic C-mode oscillations at the sonic radius of discs. *MNRAS*, 528(2):1408–1421, February 2024. <https://doi.org/10.1093/mnras/stae027>.
- Alar Toomre. On the gravitational stability of a disk of stars. *Astrophysical Journal*, vol. 139, p. 1217–1238 (1964)., 139:1217–1238, 1964.
- Peter Goldreich and D Lynden-Bell. I. gravitational stability of uniformly rotating disks. *Monthly Notices of the Royal Astronomical Society*, 130(2):97–124, 1965a.
- D. Lynden-Bell and J. P. Ostriker. On the stability of differentially rotating bodies. *MNRAS*, 136:293, January 1967. <https://doi.org/10.1093/mnras/136.3.293>.
- JCB Papaloizou and JE Pringle. The dynamical stability of differentially rotating discs-ii. *Monthly Notices of the Royal Astronomical Society*, 213(4):799–820, 1985.
- C. C. Lin and Frank H. Shu. On the Spiral Structure of Disk Galaxies, II. Outline of a Theory of Density Waves. *Proceedings of the National Academy of Science*, 55(2):229–234, February 1966. <https://doi.org/10.1073/pnas.55.2.229>.
- D Lynden-Bell and AJ Kalnajs. On the generating mechanism of spiral structure. *Monthly Notices of the Royal Astronomical Society*, 157(1):1–30, 1972.
- Bertil Lindblad. On the Dynamics of Stellar Systems (George Darwin Lecture). *MNRAS*, 108:214, January 1948. <https://doi.org/10.1093/mnras/108.3.214>.
- Peter Goldreich and Scott Tremaine. The excitation and evolution of density waves. *Astrophysical Journal*, 222(1):850–858, 1978.
- Peter Goldreich and Scott Tremaine. The excitation of density waves at the lindblad and corotation resonances by an external potential. *Astrophysical Journal*, 233(3):857–871, 1979.
- S. H. Lubow and G. I. Ogilvie. Three-dimensional Waves Generated at Lindblad Resonances in Thermally Stratified Disks. *The Astrophysical Journal*, 504(2):983, September 1998. ISSN 0004-637X. <https://doi.org/10.1086/306104>.
- Mark S Marley. Nonradial oscillations of saturn. *Icarus*, 94(2):420–435, 1991.
- MM Hedman and PD Nicholson. Kronoseismology: using density waves in saturn’s c ring to probe the planet’s interior. *The Astronomical Journal*, 146(1):12, 2013.
- Jim Fuller. Saturn ring seismology: Evidence for stable stratification in the deep interior of saturn. *icarus*, 242:283–296, 2014.
- Shoji Kato and Jun Fukue. Trapped radial oscillations of gaseous disks around a black hole. *Publications of the Astronomical Society of Japan*, Vol. 32, P. 377, 1980, 32:377, 1980.
- Shoji Kato. Low-frequency, one-armed oscillations of keplerian gaseous disks. *Astronomical Society of Japan, Publications (ISSN 0004-6264)*, vol. 35, no. 2, 1983, p. 249–261., 35:249–261, 1983.
- OM Blaes. Oscillations of slender tori. *Monthly Notices of the Royal Astronomical Society*, 216(3):553–563, 1985.
- Omer M Blaes, P Arras, and PC Fragile. Oscillation modes of relativistic slender tori. *Monthly Notices of the Royal Astronomical Society*, 369(3):1235–1252, 2006.
- Omer M Blaes, Eva Šrámková, Marek A Abramowicz, Włodek Kluźniak, and Ulf Torkelsson. Epicyclic oscillations of fluid bodies: Newtonian nonslender torus. *The Astrophysical Journal*, 665(1):642, 2007.
- George William Hill. Researches in the lunar theory. *American journal of Mathematics*, 1(1):5–26, 1878.

- Peter Goldreich and D Lynden-Bell. Ii. spiral arms as sheared gravitational instabilities. *Monthly Notices of the Royal Astronomical Society*, 130(2):125–158, 1965b.
- Shoji Kato. Pulsational instability of accretion disks to axially symmetric oscillations. *MNRAS*, 185:629–642, December 1978.  
<https://doi.org/10.1093/mnras/185.3.629>.
- P. Goldreich and S. Tremaine. Disk-satellite interactions. *ApJ*, 241:425–441, October 1980.  
<https://doi.org/10.1086/158356>.
- Steven A Balbus and John F Hawley. A powerful local shear instability in weakly magnetized disks. i-linear analysis. ii-nonlinear evolution. *Astrophysical Journal, Part 1 (ISSN 0004-637X)*, vol. 376, July 20, 1991, p. 214–233., 376:214–233, 1991.
- S. H. Lubow and J. E. Pringle. Wave Propagation in Accretion Disks: Axisymmetric Case. *The Astrophysical Journal*, 409:360, May 1993. ISSN 0004-637X.  
<https://doi.org/10.1086/172669>.
- Jeremy Goodman. A Local Instability of Tidally Distorted Accretion Disks. *ApJ*, 406:596, April 1993.  
<https://doi.org/10.1086/172472>.
- D. G. Korycansky and J. E. Pringle. Axisymmetric waves in polytropic accretion discs. *Monthly Notices of the Royal Astronomical Society*, 272(3):618–624, February 1995. ISSN 0035-8711.  
<https://doi.org/10.1093/mnras/272.3.618>.
- G.I. Ogilvie. Waves and instabilities in a differentially rotating disc containing a poloidal magnetic field. *Monthly Notices of the Royal Astronomical Society*, 297(1):291–314, June 1998. ISSN 0035-8711.  
<https://doi.org/10.1046/j.1365-8711.1998.01507.x>.
- Steven A Balbus and John F Hawley. Instability, turbulence, and enhanced transport in accretion disks. *Reviews of modern physics*, 70(1):1, 1998.
- G. I. Ogilvie and S. H. Lubow. The Effect of an Isothermal Atmosphere on the Propagation of Three-dimensional Waves in a Thermally Stratified Accretion Disk. *The Astrophysical Journal*, 515(2):767, April 1999. ISSN 0004-637X. <https://doi.org/10.1086/307037>.
- Andrew N Youdin and Jeremy Goodman. Streaming instabilities in protoplanetary disks. *The Astrophysical Journal*, 620(1):459, 2005.
- Anders Johansen, Jeffrey S Oishi, Mordecai-Mark Mac Low, Hubert Klahr, Thomas Henning, and Andrew Youdin. Rapid planetesimal formation in turbulent circumstellar disks. *Nature*, 448(7157):1022–1025, 2007.
- Richard P Nelson, Oliver Gressel, and Orkan M Umurhan. Linear and non-linear evolution of the vertical shear instability in accretion discs. *Monthly Notices of the Royal Astronomical Society*, 435(3):2610–2632, 2013.
- Conny Aerts, Jørgen Christensen-Dalsgaard, and Donald W. Kurtz. *Asteroseismology*. 2010.  
<https://doi.org/10.1007/978-1-4020-5803-5>.
- Pierre Delplace, JB Marston, and Antoine Venaille. Topological origin of equatorial waves. *Science*, 358(6366):1075–1077, 2017.
- Manolis Perrot, Pierre Delplace, and Antoine Venaille. Topological transition in stratified fluids. *Nature Physics*, 15(8):781–784, 2019.
- Nicolas Perez, Pierre Delplace, and Antoine Venaille. Unidirectional modes induced by nontraditional coriolis force in stratified fluids. *Physical Review Letters*, 128(18):184501, 2022.
- Jeffrey B Parker, JB Marston, Steven M Tobias, and Ziyang Zhu. Topological gaseous plasmon polariton in realistic plasma. *Physical Review Letters*, 124(19):195001, 2020.
- Hong Qin and Yichen Fu. Topological langmuir-cyclotron wave. *Science Advances*, 9(13):eadd8041, 2023.
- Nicolas Perez, Armand Leclerc, Guillaume Laibe, and Pierre Delplace. Topology of shallow-water waves on a rotating sphere. *Journal of Fluid Mechanics*, 1003:A35, January 2025. <https://doi.org/10.1017/jfm.2024.1228>.
- Armand Leclerc, Guillaume Laibe, Pierre Delplace, Antoine Venaille, and Nicolas Perez. Topological modes in stellar oscillations. *The Astrophysical Journal*, 940(1):84, 2022.
- Armand Leclerc, Lucien Jezequel, Nicolas Perez, Asmita Bhandare, Guillaume Laibe, and Pierre Delplace. Exceptional ring of the buoyancy instability in stars. *Physical Review Research*, 6(1):L012055, March 2024a.  
<https://doi.org/10.1103/PhysRevResearch.6.L012055>.
- Arthur Le Saux, Armand Leclerc, Guillaume Laibe, Pierre Delplace, and Antoine Venaille. A Core-sensitive Mixed f/g-mode of the Sun Predicted by Wave Topology and Hydrodynamical Simulation. *ApJL*, 987(1):L12, July 2025. <https://doi.org/10.3847/2041-8213/ade396>.
- Armand Leclerc, Guillaume Laibe, and Nicolas Perez. Wave topology of stellar inertial oscillations. *Physical Review Research*, 6(4):043299, December 2024b.  
<https://doi.org/10.1103/PhysRevResearch.6.043299>.
- Stefan Keppeler. Introduction to wigner-weyl calculus, 2004. URL <https://www.math.uni-tuebingen.de/user/stke/teaching/wigner-weyl>.
- Brian C Hall. *Quantum theory for mathematicians*. Springer, 2013.



- Yohei Onuki. Quasi-local method of wave decomposition in a slowly varying medium. *Journal of Fluid Mechanics*, 883:A56, 2020.
- Jérémie Vidal and Yves Colin de Verdière. Inertia-gravity waves in geophysical vortices, 2024.
- Henrik N Latter and John Papaloizou. Local models of astrophysical discs. *Monthly Notices of the Royal Astronomical Society*, 472(2):1432–1446, 2017.
- Min-Kai Lin and Andrew N Youdin. Cooling requirements for the vertical shear instability in protoplanetary disks. *The Astrophysical Journal*, 811(1):17, 2015.
- Grigory E Volovik. *The universe in a helium droplet*, volume 117. OUP Oxford, 2003.
- Pierre Delplace. Berry-chern monopoles and spectral flows. *SciPost Physics Lecture Notes*, page 039, 2022.
- Frédéric Faure. Manifestation of the topological index formula in quantum waves and geophysical waves. *Annales Henri Lebesgue*, 6:449–492, 2023.
- Keita Iga. Transition modes in stratified compressible fluids. *Fluid dynamics research*, 28(6):465, 2001.
- Philip J Armitage. Dynamics of protoplanetary disks. *Annual Review of Astronomy and Astrophysics*, 49: 195–236, 2011.
- Keaton J Burns, Geoffrey M Vasil, Jeffrey S Oishi, Daniel Lecoanet, and Benjamin P Brown. Dedalus: A flexible framework for numerical simulations with spectral methods. *Physical Review Research*, 2(2):023068, 2020.
- Jeffrey S Oishi, Keaton J Burns, Susan E Clark, Evan H Anders, Benjamin P Brown, Geoffrey M Vasil, and Daniel Lecoanet. eigentools: A python package for studying differential eigenvalue problems with an emphasis on robustness. *Journal of Open Source Software*, 6(62):3079, 2021.
- Sean M Andrews, Jane Huang, Laura M Pérez, Andrea Isella, Cornelis P Dullemond, Nicolás T Kurtovic, Viviana V Guzmán, John M Carpenter, David J Wilner, Shangjia Zhang, et al. The disk substructures at high angular resolution project (dsharp). i. motivation, sample, calibration, and overview. *The Astrophysical Journal Letters*, 869(2):L41, 2018.
- M. Abramowitz and I. A. Stegun. *Handbook of Mathematical Functions*. US Department of Commerce, 1972.
- RVE Lovelace, H Li, SA Colgate, and AF Nelson. Rossby wave instability of keplerian accretion disks. *The Astrophysical Journal*, 513(2):805, 1999.
- Jonathan Squire and Philip F. Hopkins. Resonant drag instabilities in protoplanetary discs: the streaming instability and new, faster growing instabilities. *MNRAS*, 477(4):5011–5040, July 2018. <https://doi.org/10.1093/mnras/sty854>.
- V. V. Zhuravlev. On the nature of the resonant drag instability of dust streaming in protoplanetary disc. *MNRAS*, 489(3):3850–3869, November 2019. <https://doi.org/10.1093/mnras/stz2390>.
- Marius Lehmann and Min-Kai Lin. Instabilities in dusty non-isothermal protoplanetary discs. *MNRAS*, 522(4): 5892–5930, July 2023. <https://doi.org/10.1093/mnras/stad1349>.
- Sijme-Jan Paardekooper and Hossam Aly. Resonant drag instabilities for polydisperse dust: II. The streaming and settling instabilities. *A&A*, 697:A40, May 2025. <https://doi.org/10.1051/0004-6361/202453496>.
- Shoji Kato. Resonant Excitation of Disk Oscillations by Warps: A Model of kHz QPOs. *PASJ*, 56:905–922, October 2004. <https://doi.org/10.1093/pasj/56.5.905>.
- Shoji Kato. Resonant Excitation of Disk Oscillations in Deformed Disks II: A Model of High-Frequency QPOs. *PASJ*, 60:111, February 2008. <https://doi.org/10.1093/pasj/60.1.111>.
- Bárbara T. Ferreira and Gordon I. Ogilvie. On an excitation mechanism for trapped inertial waves in discs around black holes. *MNRAS*, 386(4):2297–2310, June 2008. <https://doi.org/10.1111/j.1365-2966.2008.13207.x>.
- Janosz W. Dewberry, Henrik N. Latter, and Gordon I. Ogilvie. Quasi-periodic oscillations and the global modes of relativistic, MHD accretion discs. *MNRAS*, 476(3): 4085–4103, May 2018. <https://doi.org/10.1093/mnras/sty385>.
- Benoît Commerçon, Francesco Lovascio, Elliot Lynch, and Enrico Ragusa. Discs are born eccentric. *A&A*, 689:L9, September 2024. <https://doi.org/10.1051/0004-6361/202449610>.
- S. H. Lubow and G. I. Ogilvie. Secular Interactions between Inclined Planets and a Gaseous Disk. *ApJ*, 560 (2):997–1009, October 2001. <https://doi.org/10.1086/322493>.
- Jean Teyssandier and Gordon I. Ogilvie. Growth of eccentric modes in disc-planet interactions. *MNRAS*, 458 (3):3221–3247, May 2016. <https://doi.org/10.1093/mnras/stw521>.
- Atsuo T Okazaki, Shoji Kato, and Jun Fukue. Global trapped oscillations of relativistic accretion disks. *Publications of the Astronomical Society of Japan*, 39(3): 457–473, 1987.

Wolfram Research, Inc. Mathematica, Version 14.0, 2024.  
URL <https://www.wolfram.com/mathematica>.  
Champaign, IL.

## APPENDIX

## A. CONSTANT OF MOTION

The evolution equation of the perturbations  $X(r, k_z, t)$  is

$$i\partial_t X = \mathcal{H}X. \quad (\text{A1})$$

As  $\mathcal{H}$  is self-adjoint with respect to the inner product

$$\langle X, Y \rangle = \int dr X^{\top*} \cdot Y, \quad (\text{A2})$$

where  $\cdot$  is the matricial product, such that  $\langle X, \mathcal{H}Y \rangle = \langle \mathcal{H}X, Y \rangle$  for boundary conditions with zero radial velocity. One then has

$$i\partial_t \langle X, X \rangle = \langle -i\partial_t X, X \rangle + \langle X, i\partial_t X \rangle, \quad (\text{A3})$$

$$= -\langle \mathcal{H}X, X \rangle + \langle X, \mathcal{H}X \rangle, \quad (\text{A4})$$

$$= -\langle X, \mathcal{H}X \rangle + \langle X, \mathcal{H}X \rangle, \quad (\text{A5})$$

$$= 0. \quad (\text{A6})$$

$I = \frac{1}{2} \langle X, X \rangle$  is then a constant of motion, given by the self-adjointness of the evolution operator  $\mathcal{H}$ . Equation (15) gives it in dimensional form, where one reads that it is a pseudo-energy of the wave, as the sum of kinetic and pressure energy contributions.

B. SELF-ADJOINTNESS OF  $\mathcal{H}$ 

We show here that  $\mathcal{H}$  is self-adjoint on the Hilbert space  $\{X = \begin{pmatrix} u_z & u_r & u_\theta & h \end{pmatrix}^\top, u_r(r_0) = u_r(r_1) = 0\}$  with respect to the canonical inner product  $\langle X_1, X_2 \rangle = \int dr X_1^* X_2$ .

$$\langle X_1, \mathcal{H}X_2 \rangle = \int dr \left( c_s k_z (u_{z,1}^* h_2 + h_1^* u_{z,2}) + i\kappa (u_{\theta,1}^* u_{r,2} - u_{r,1}^* u_{\theta,2}) \right) \quad (\text{B7})$$

$$+ \int dr u_{r,1}^* \left( ic_s \partial_r h_2 + i \frac{c_s'}{2} h_2 - iSh_2 \right) + \int dr h_1^* \left( ic_s \partial_r u_{r,2} + i \frac{c_s'}{2} u_{r,2} + iSu_{r,2} \right),$$

$$= \int dr \left( c_s k_z (u_{z,1}^* h_2 + h_1^* u_{z,2}) + i\kappa (u_{\theta,1}^* u_{r,2} - u_{r,1}^* u_{\theta,2}) \right) \quad (\text{B8})$$

$$+ [ic_s u_{r,1}^* h_2] - \int dr \left( ic_s \partial_r u_{r,1}^* + i \frac{c_s'}{2} u_{r,1}^* + iSu_{r,1}^* \right) h_2 + [ic_s h_1^* u_{r,2}] - \int dr \left( ic_s \partial_r h_1^* + i \frac{c_s'}{2} h_1^* - iSh_1^* \right) u_{r,2},$$

$$= \int dr \left( (c_s k_z u_{z,1})^* h_2 + (c_s k_z h_1)^* u_{z,2} + (-i\kappa u_{\theta,1})^* u_{r,2} + (i\kappa u_{r,1})^* u_{\theta,2} \right) \quad (\text{B9})$$

$$+ [ic_s u_{r,1}^* h_2] + \int dr \left( ic_s \partial_r u_{r,1} + i \frac{c_s'}{2} u_{r,1} + iSu_{r,1} \right)^* h_2 + [ic_s h_1^* u_{r,2}] + \int dr \left( ic_s \partial_r h_1 + i \frac{c_s'}{2} h_1 - iSh_1 \right)^* u_{r,2},$$

$$= \langle \mathcal{H}X_1, X_2 \rangle + [ic_s (u_{r,1}^* h_2 + h_1^* u_{r,2})]. \quad (\text{B10})$$

The bracket term goes to zero for impenetrable boundaries.  $\mathcal{H}$  is therefore self-adjoint.

## C. PROFILES OF MODES

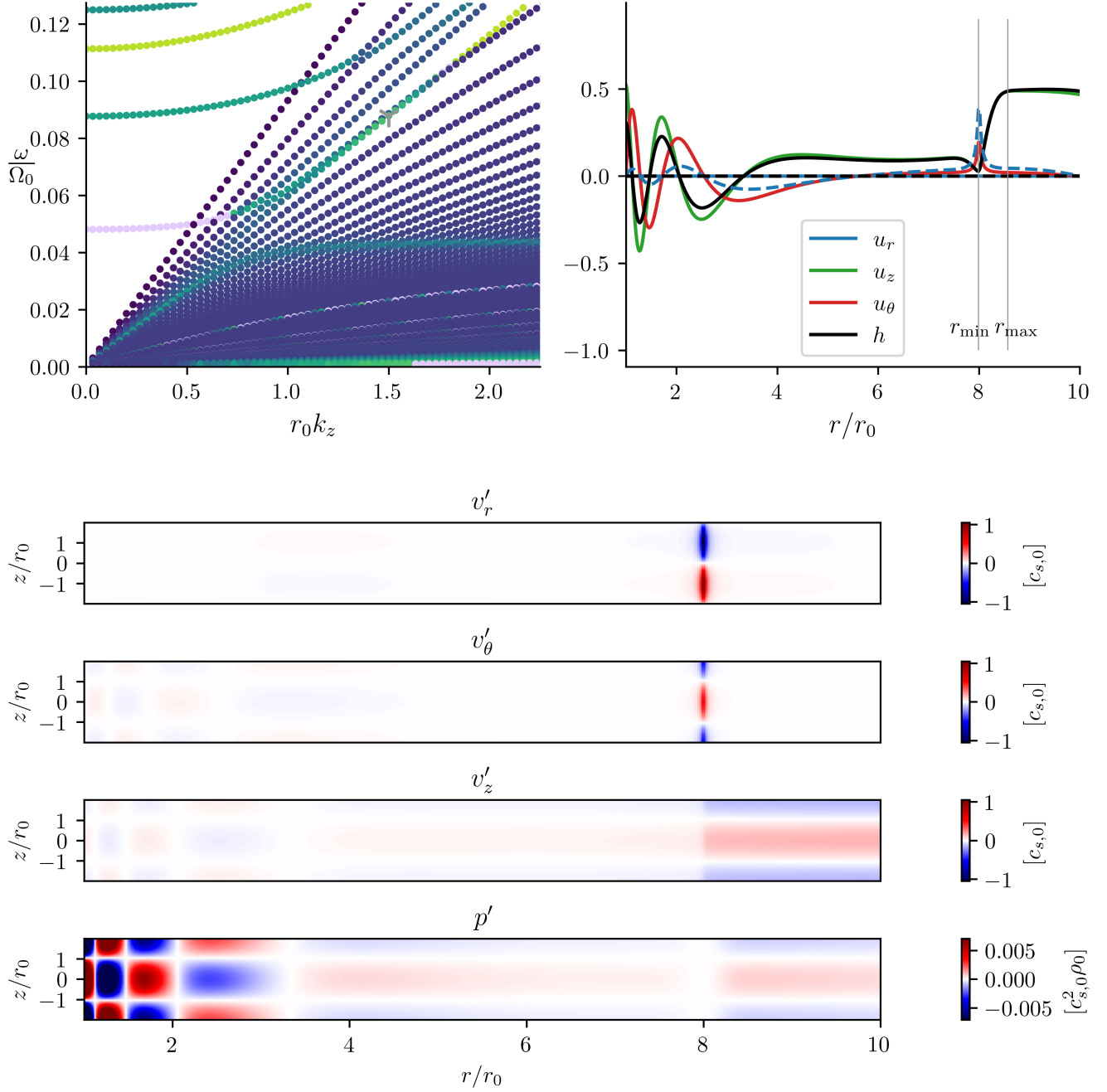


**Figure 6.** Relative amplitudes of the components of a fundamental  $p$ -mode with large  $k_z$ , of topological origin, induced by a pressure bump located close to  $r_{\max}$ . The amplitudes are displayed as functions of the distance to the central object in the mid-plane (top right panel) and for a  $(r, z)$  slice of the disc (bottom panel). The selected mode is marked with a cross in the top left panel (same as Fig. 2). This mode colored red have amplitudes(?) in  $(u_z, h)$  and as such, is of acoustic nature. Interestingly, it mixes with both the fundamental  $r$ -mode of the gap and an inertial mode of the inner disc, which both have amplitudes in  $u_r$  and  $u_\theta$ . It is more spatially extended around  $r_{\max}$  than the fundamental  $r$ -mode is around  $r_{\min}$  (see below).



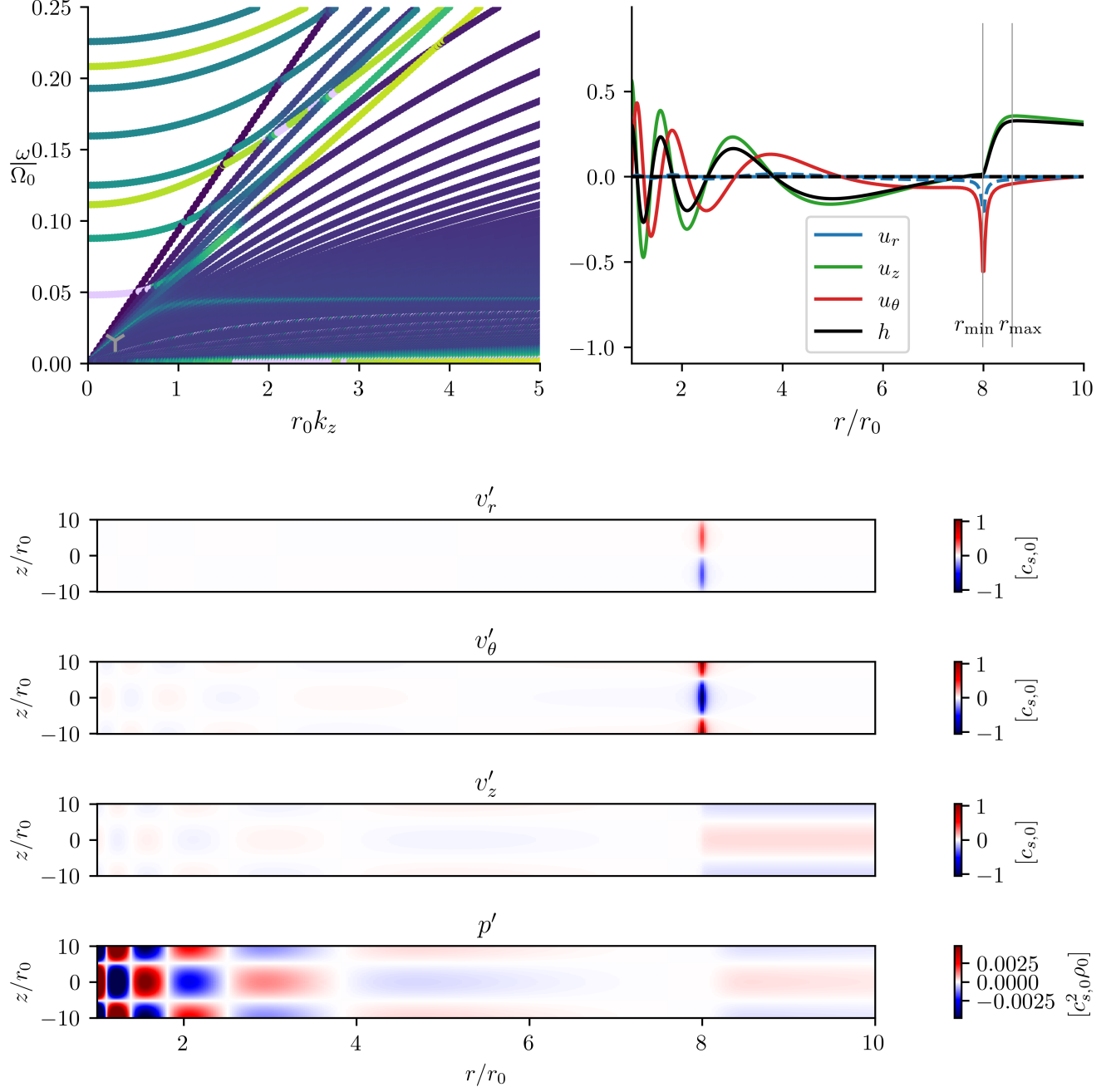


**Figure 7.** Same as Fig. 6, but for a mode a low  $k_z$  (note the different  $z$  scale). The properties of this mode are similar to the one displayed in Fig. 6.

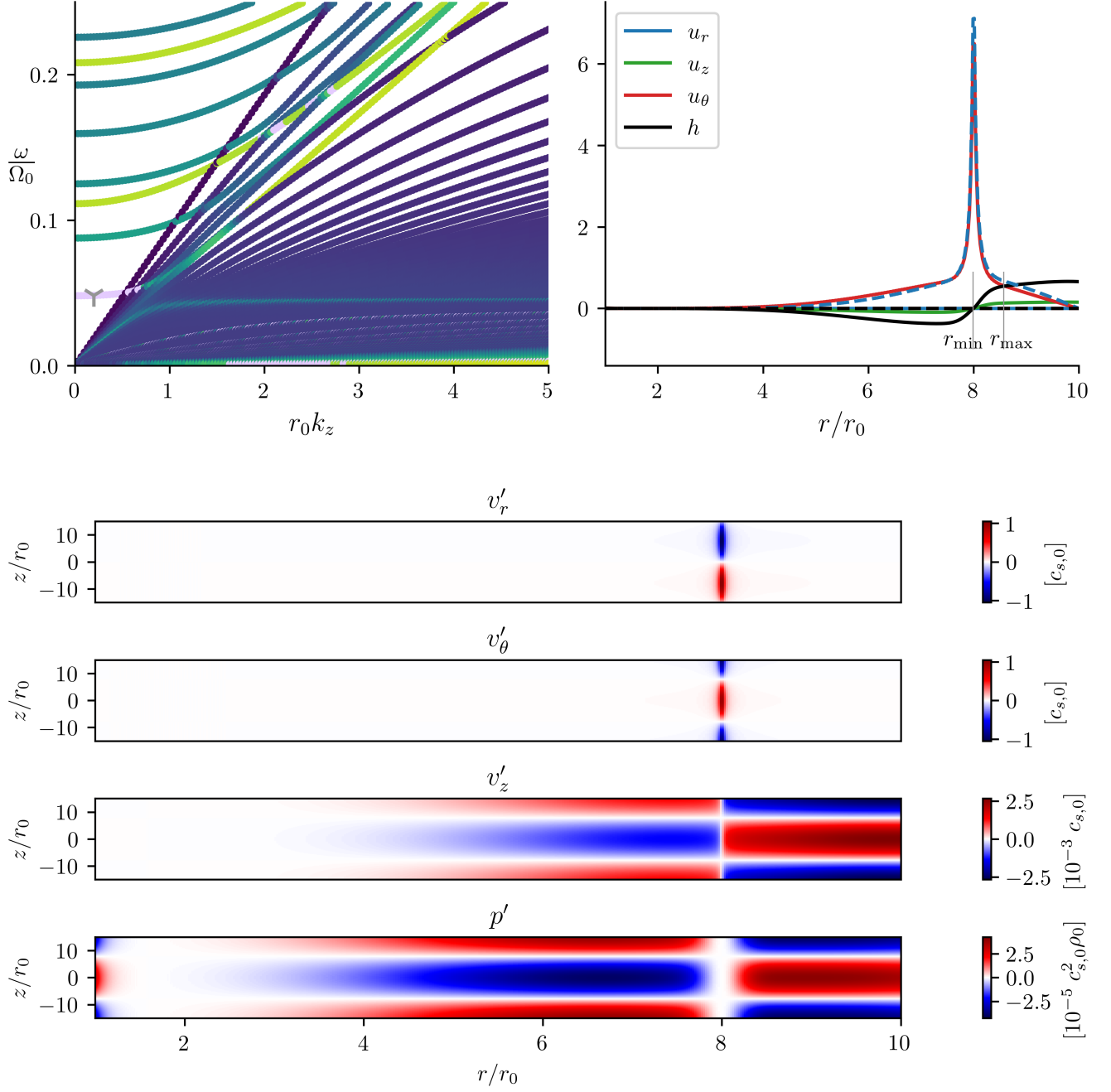


**Figure 8.** Same as Fig. 6 for the the fundamental  $r$ -mode, topologically induced by the existence of the a pressure gap. The mode exhibits strong horizontal motions around  $r_{\min}$  (note the scales colorbars), where the amplitude peaks. The mode extends outwards of the gap, and has non-zero amplitude at  $r_{\max}$ , where grains may eventually pile-up. The mode mixes with acoustic vibrations outside of  $r_{\min}$ .

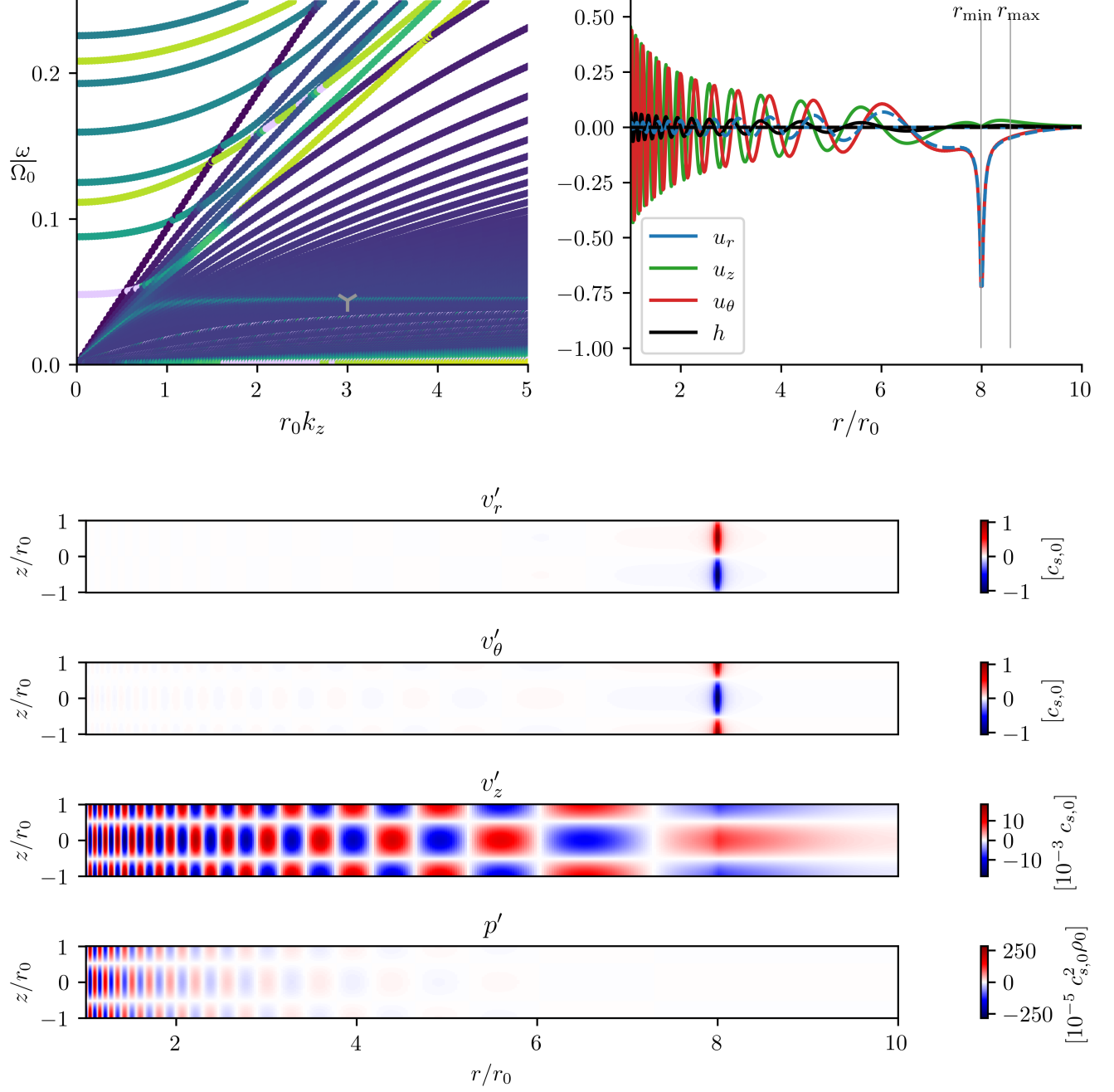


**Figure 9.** Same as Fig. 8, but for larger values of  $k_z$  (note the different scale on  $z$ ). The fundamental vibration of the gap couples with an inertial vibration of the rest of the disc, such that vertical motions have comparable amplitudes with horizontal motions within the gap (note the scales colorbars).

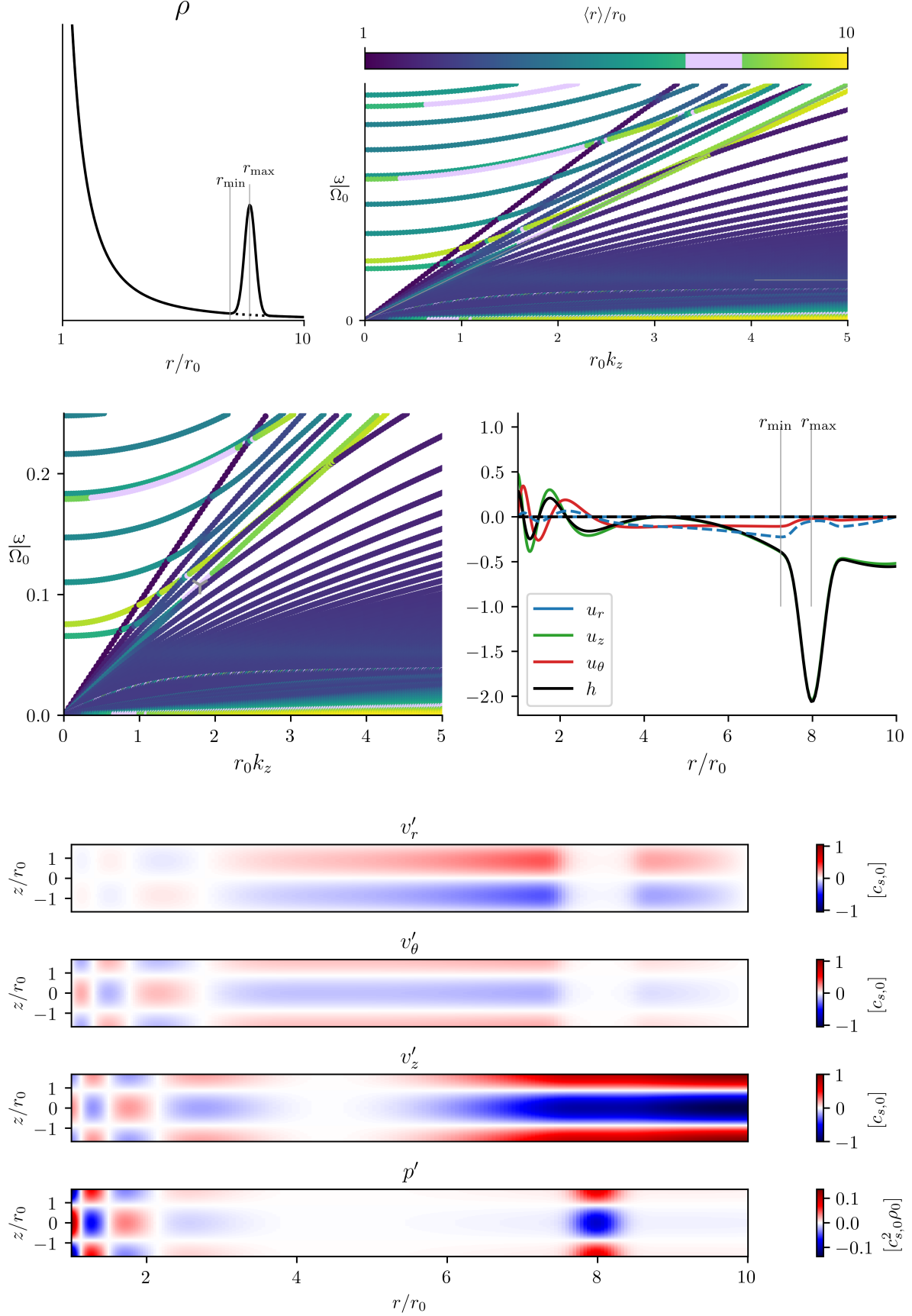


**Figure 10.** Same as Fig. 6, but for a disc having a pressure bump. The parameters of the bump are similar to the ones used to parametrize the gap, with a reversed amplitude  $A = -20$ . The mode is essentially of acoustic nature, while it mixes with inertial modes in the inner regions. The inertial topological mode associated to the presence of a pressure minimum at the inner edge is present, but difficult to distinguish since it is very delocalized.